Journal of the American Heart Association

ORIGINAL RESEARCH

Single-Cell Transcriptome Profiling Reveals Dynamic Cell Populations and Immune Infiltration in Moyamoya Disease

Shihao He, MD, PhD;* Junze Zhang, MD, PhD;* Zhenyu Zhou, MD;* Zhen Qi, PhD; Xilong Wang, MD; Yanru Wang, MD; Yutong Liu, MD; Yunqing Zhou, BS; Chengxu Lei, MD; Xun Ye, MD, PhD; Yuanli Zhao, MD, PhD

BACKGROUND: The cellular composition and molecular mechanisms of the pathological arteries in Moyamoya disease (MMD) remain poorly understood. To improve our understanding of pathogenesis in MMD, we aimed to comprehensively map the cellular composition and molecular alterations within the pathological arteries of patients with MMD.

METHODS: Superficial temporal artery samples were collected from patients with MMD (n=2) and healthy controls (n=3), yielding a total of 26 371 cells that were used for single-cell RNA sequencing. Differentially expressed genes, pathway enrichment, and cell–cell communication analyses were performed to examine disease-related changes. In vitro experiments were performed to validate the changes in endothelial cells (ECs) and smooth-muscle cells (SMCs), as well as the interactions between immune cells and ECs and SMCs.

RESULTS: We identified 8 major cell types in the human superficial temporal artery. We observed an increased proportion of SMCs in the superficial temporal artery of MMD. Two distinct SMC clusters, SMC1 and SMC2, were identified and exhibited different gene expression. Immune profiling revealed significant upregulation of genes in natural killer T cells, suggesting increased immune activity in MMD. Cell–cell communication analysis highlighted the role of the macrophage migration inhibitory factor pathway in promoting interactions between immune cells, SMCs, and ECs. In vitro experiments confirmed that the colocalization of CD74 with CD44 or CXCR4 in ECs promotes EC proliferation and angiogenesis. Natural killer T cells can promote cytoskeletal enlargement in ECs and SMCs, enhancing their migratory and proliferative capacities, as well as promoting angiogenesis in ECs.

CONCLUSIONS: This study provides a single-cell transcriptomic map of the superficial temporal artery in MMD, revealing key immune and vascular cell populations. Immune cells, particularly natural killer T cells, play a critical role in promoting SMC and EC proliferation and migration, contributing to vascular occlusion. These findings make contributions to understanding the pathogenesis of MMD and suggest potential therapeutic targets.

Key Words: endothelial cells ■ immune infiltration ■ Moyamoya disease ■ single-cell RNA sequencing

Moyamoya disease (MMD) is a rare chronic cerebrovascular disease, the main features of which are progressive occlusion of internal carotid artery and abnormal vascular network formation.[1,2] The histological characteristics of the pathological arteries are the thickening of the intima, irregular undulation of

Correspondence to: Shihao He, MD, PhD and Yuanli Zhao, MD, PhD, Department of Neurosurgery, Peking Union Medical College Hospital, Peking Union Medical College and Chinese Academy of Medical Sciences, No.1 Shuaifuyuan, Dongcheng District, Beijing 100730, China. Email: heshihaoo@outlook.com and zhaoyuanli@126.com and Xun Ye, MD, PhD, Department of Neurosurgery, Beijing Tiantan Hospital, Capital Medical University; No.119 South 4th Ring West Road, Fengtai District, Beijing 100070, China. Email: yexun79@hotmail.com

*S. He, J. Zhang, and Z. Zhou are co-first authors.

This manuscript was sent to Neel Singhal, MD, PhD, Associate Editor, for review by expert referees, editorial decision, and final disposition.

Supplemental Material is available at https://www.ahajournals.org/doi/suppl/10.1161/JAHA.124.041168

For Sources of Funding and Disclosures, see page 17.

JAHA is available at: www.ahajournals.org/journal/jaha

RESEARCH PERSPECTIVE

What Is New?

- Single-cell RNA sequencing of superficial temporal arteries from patients with moyamoya disease delineates 2 metabolically distinct smooth-muscle clusters and 4 endothelial subsets, revealing selective expansion of a hyperproliferative smooth-muscle cell population that drives intimal thickening.
- The data uncover immune-vascular crosstalk in which infiltrating natural killer T cells, acting through migration inhibitory factor–CD74/CD44 and migration inhibitory factor–CD74/CXCR4 signaling, promote cytoskeletal enlargement, migration, proliferation and angiogenic activity of both smooth-muscle cells and endothelial cells.

What Question Should Be Addressed Next?

- The next priorities are to elucidate moyamoya-specific immune pathways and evaluate whether therapeutic blockade of the migration inhibitory factor–CD74 axis or modulation of natural killer T-cell activity can halt smooth-muscle phenotypic switching and prevent progressive arterial stenosis in moyamoya and related occlusive vasculopathies.

Nonstandard Abbreviations and Acronyms

DEG	differentially expressed gene
EC	endothelial cell
HBMEC	human brain microvascular endothelial cell
HBVSMC	human brain vascular smooth-muscle cell
HC	healthy control
MIF	migration inhibitory factor
MMD	moyamoya disease
NKT	natural killer T
sc-RNAseq	single-cell RNA sequencing
SMC	smooth-muscle cell
STA	superficial temporal artery
UMI	unique molecular identifier
VSMCs	vascular smooth-muscle cell

internal elastic lamina, thinner media, and pathologically increased angiogenesis.[3–5] Recently in the field of MMD, many studies have provided pathological evidence on the involvement of vascular smooth-muscle cell (VSMC) and endothelial cell (EC) proliferation and migration in vascular stenosis.[6–8] However, the molecular and cellular mechanisms leading to these pathological changes of MMD vessels remain poorly understood.

Single-cell RNA sequencing (sc-RNAseq) enables unbiased, high-throughput, and high-resolution transcriptomic analysis of individual cells. It can recognize intercell variability, identify complex cell populations, and reveal regulatory relationships between genes.[9,10] Li et al[11] performed sc-RNAseq analysis of ascending aortic tissues from 11 study participants, and 11 major cell types were identified. By comparing ascending thoracic aortic aneurysm and control tissues, the erythroblast transformation–specific related gene was found to play an important role in maintaining normal aortic wall function. In addition, this study revealed the cellular and molecular map of the human ascending aorta at the single-cell level, expanding the understanding of the mechanism of aortic aneurysm. Li et al[12] conducted sc-RNAseq on venous malformation and cavernous venous malformation and found that the proportion of immune cells such as macrophages and monocytes increased abnormally to 30%. In addition, combined with gene set enrichment analysis, it was found that inflammatory pathways, innate immune response, and angiogenic signaling pathways were abnormally activated in the pathogenesis of venous malformation and cavernous venous malformation. The identification of cells and cell subtypes in this study provides key pathological evidence for immune-related mechanisms regulating the growth of vascular malformations. Similarly, sc-RNAseq has greatly advanced the understanding of the molecular mechanisms of various diseases by mapping genes at the level of individual cells.

The heterogeneity and function of arterial cell types are critical for pathological processes of arteries in vascular diseases.[13,14] In vascular diseases, phenotype transformation of VSMCs driven by metabolic pathways is a characteristic pathological change of vascular injury.[15] A study using sc-RNAseq and fate mapping of VSMCs has revealed the transition and regression of multiple VSMC phenotypes in atherosclerosis. It was first proposed that all-trans retinoic acid could reduce atherosclerosis load by inhibiting SMC phenotypic transition, which was confirmed by in vitro experiments.[16] However, it is difficult to acquire and sequence pathological arterioles in patients with MMD. In a study that included 2 patients with MMD and 4 normal controls, peripheral blood of the participants was sequenced by sc-RNAseq and individual cell landscape of MMD peripheral blood was provided. In addition, by combining weighted correlation network analysis and cell interaction analysis, the potential hub genes and immune cells of MMD were obtained.[17] But the blood cannot directly represent the cellular characteristics of the MMD arteries. The lack of identification

and grouping of VSMCs and ECs has limited the exploration of the mechanism of pathological changes of MMD arteries. Therefore, identifying the cell-specific changes of MMD arteries through sc-RNAseq of vascular tissue will greatly contribute to understanding the pathogenesis of MMD.

In this study, we collected the superficial temporal artery (STA) specimens from patients with MMD and performed sc-RNAseq to characterize the cellular heterogeneity of STA from patients with MMD and controls. We identified 22 cell subpopulations, including 8 major cell types such as ECs and SMCs. To reveal the roles of these cell types in the pathogenesis of MMD, we also performed the analyses of differential gene expresssion, pathway enrichment, and cell communication. Our analysis revealed an increased proportion of SMCs in the STA of patients with MMD and identified distinct gene expression profiles of SMCs and immune cells between patients with MMD and healthy controls (HCs). Bioinformatics analysis and in vitro experiments revealed that immune cells in MMD, particularly natural killer T (NKT) cells, promote the proliferation, migration, and cytoskeletal enlargement of ECs and SMCs, which may play role in the intimal thickening of the diseased arteries. These findings expand our understanding of the cellular composition of diseased arteries and the pathogenesis of MMD, contributing to the exploration of potential treatment approaches in the future.

METHODS

The data that support the findings of this study are available from the corresponding author upon reasonable request. Specific methods used in this study can be found in Data S1.

Enrollment of Study Participants and Collection of Tissue Samples

Patients with MMD were clinically diagnosed by medical history and neuroradiological examination following the diagnostic guidelines.[2] STA (1–3 mm) samples were obtained during direct or combined revascularization surgery of patients with MMD. Control STA samples were obtained during craniotomy from patients undergoing epilepsy surgery. Clinical and imaging data were obtained from medical records and picture archiving and communication systems, respectively. The protocol for collecting human tissue samples was approved by Institutional Ethics Committee of Peking Union Medical College Hospital. Written informed consent was obtained from all participants (parents/guardians of patients aged <18 years) before the study. This study was approved by the Institutional Ethics Committee of Peking Union Medical College Hospital, Beijing, China (I-24YSB0160).

Single-Cell RNA Sequencing and Data Analysis

Single-cell suspensions were processed through the 10x Genomics Chromium System (10x Genomics, Pleasanton, CA) to generate 3′ gene expression libraries the Chromium Single Cell 3′ Reagent Kit v3 (10x Genomics). Briefly, single-cell suspensions, along with reagents, gel beads, and partitioning oil, were loaded onto a 10x Chromium Chip B. In the chip, each individual cell was encapsulated in an oil droplet that contained gel beads and reagents, creating a gel bead in emulsion. Each gel bead in emulsion provides an independent reaction space for the cell, where the primers on the gel beads include a sequencing primer, a cell-specific barcode, unique molecular identifiers (UMIs), and a poly(deoxythymidine) tail. Inside each gel bead in emulsion, the cell was lysed, and polyadenylated mRNA was reverse transcribed into barcoded full-length cDNA. All cDNA molecules were then pooled, followed by general library construction steps, including amplification, fragmentation, end repair, adapter ligation, and sample index polymerase chain reaction. The resulting libraries were sequenced on a NovaSeq 6000 platform (Illumina Inc., San Diego, CA), with paired-end sequencing using the PE150 strategy. A target depth of 50 000 to 100 000 reads per cell was achieved, corresponding to a total data output of 15 to 30 million reads per sample.

After obtaining the raw sequenced reads, the data were processed using 10x Genomics' Cell Ranger software for cell barcode and UMI counting and for gene expression matrix generation. The generated gene-specific UMI count matrix was analyzed using the Seurat R package version 4.3.0.1 (R Foundation for Statistical Computing, Vienna, Austria). We retained only cells that expressed at least 500 genes and genes that were expressed in at least 50 cells. Cells were further filtered by a maximum of 5500 expressed genes and 5% mitochondrial gene content, resulting in the selection of 26 371 cells for subsequent analysis. The UMI counts for each cell were then normalized to total expression, multiplied by 10 000, and log-transformed. We used the default method in Seurat to identify highly variable genes and scaled and regressed UMI data and mitochondrial genes using the ScaleData function. Principal component analysis was performed using the highly variable genes. The most significant principal components were identified using the ElbowPlot function, and 19 principal component analysis components were selected for downstream analysis, including clustering and identification of cell populations. Uniform manifold approximation and projection was computed in the Seurat R package using the top 19 principal component analysis components with mindist set to 0.75. Batch effect removal and correction

were performed using the Harmony package. We used the DoubleFinder package to assess potential doublets in the data set. Based on the recommendations from 10x Genomics at the single-cell level, a threshold of 7.5% was chosen as the cutoff for doublet formation. Additionally, for each cluster, those that showed significant enrichment of highly expressed genes across markers from ≥2 cell types were also considered doublet clusters and were removed from further analysis.

Cell Clustering and Annotation

After removing doublets, we reidentified highly variable genes and performed principal component analysis analysis on the data set, followed by uniform manifold approximation and projection for dimensionality reduction. We conducted cell clustering analysis using the FindNeighbors and FindClusters functions, determining that a resolution of 0.3 was the optimal clustering parameter. To annotate each cell type, we referenced previously identified cell markers for annotation, such as endothelial cells ("FLT1," "CLDN"), fibroblasts ("COL1A1," "COL3A1," "FAP," "THY1"), pericytes ("TAGLN"), microglia ("TYROBP," "CSF1R," "CD74"), oligodendrocytes ("APOD"), vascular-associated oligodendrocytes ("PLP1"), and T lymphocytes ("CD3D," "CD69"). Subsequently, we identified markers for cell subpopulations using the FindAllMarkers package, and statistical testing was performed using the Wilcox test. Genes with $P<0.05$ and avg_Log2FC>0.25 were selected for gene ontology and Kyoto Encyclopedia of Genes and Genomes enrichment analysis to identify the activated pathways for each cell subtype. Functional and pathway enrichment, including Kyoto Encyclopedia of Genes and Genomes and gene ontology analyses, were conducted using the ClusterProfiler package version 3.8.1.

Statistical Analysis

Statistical analyses were conducted using Prism version 9.4.0 (GraphPad Software, La Jolla, CA). Results are presented as means±SD. An independent sample Student's *t* test was applied for comparisons between 2 groups. For comparisons among >2 groups, 1-way ANOVA followed by Tukey's post hoc test was used. A *P* value of <0.05 was considered statistically significant, with all *P* values being 2-tailed. For bulk RNA sequencing differential expression analysis, *P* values were adjusted for multiple hypothesis testing using the Benjamini–Hochberg method to control the false discovery rate, and genes with adjusted *P* values <0.05 were considered significant.

RESULTS

Gene Profiles of 8 Major Cell Types in Human STA Tissues in Patients With MMD and HCs

We obtained 2 STA samples intraoperatively from 2 patients with MMD (1 man and woman) undergoing revascularization surgery. As controls, we collected non-diseased STA samples intraoperatively from 3 patients with epilepsy (men) undergoing surgery. After quality control, a total of 26371 single cells were obtained and subsequently used for sc-RNAseq (Figure 1A). Data from the 5 samples were then integrated using the Seurat R package. After integrating all the samples, the cells were clustered into 21 distinct subpopulations. After examining conserved genes in each cluster, we obtained 8 major cell types in the STA samples by merging the cell clusters with similar gene expression profiles (Figure 1B). The 8 major cell types included lymphocyte, endotheliocyte, fibrocyte, oligodendrocyte, SMC, pericyte, microglial, and some unidentified cells. The summary of captured cell numbers and cell types for each sample is listed in Table S1. Among them, the SMCs were primarily divided into 2 subpopulations, SMC1 and SMC2, with SMC1 upregulated in MMD, associated with blood vessel regulation, and SMC2 involved in transmembrane transport. The proportion of each cell subtypes within each STA sample was shown in Figure 1C. A comprehensive comparison of cell types between MMD and HC STA samples revealed a significant increase in the proportion of SMCs within the vascular wall of MMD samples (Figure 1D). Each cell type showed a distinct gene expression profile (Figure 1E and 1F). To determine which cell types were most transcriptionally affected in MMD, we also performed differentially expressed gene (DEG) analysis for each of the 8 major cell types (Figures S1 through S5).

Different Clusters and Heterogeneity of SMC and EC Populations in Human Superficial Temporal Artery Tissues

Among the 21 distinct subpopulations, we identified 2 kinds of SMC clusters. SMC1 and SMC2

Figure 1. Nineteen major cell types identified with single-cell RNA sequencing analysis of STA tissues.
A, Schematic diagram of the sample collection and single-cell sequencing workflow. **B**, UMAP plot of all cells colored according to the 11 major cell types. **C**, Bar plot showing the proportion of each cell type from all STA samples. **D**, Bar plot showing the composition of each cell type between MMD and HC STA samples. **E**, UMAP plot showing the relative expression of several marker genes in all cells from all STA samples. **F**, Bar plot showing the relative expression of several marker genes in all cells from all STA samples. HC indicates healthy control; MMD, moyamoya disease; sc-RNAseq, single-cell RNA sequencing; SMC, smooth-muscle cell; STA, superficial temporal artery; and UMAP, uniform manifold approximation and projection.

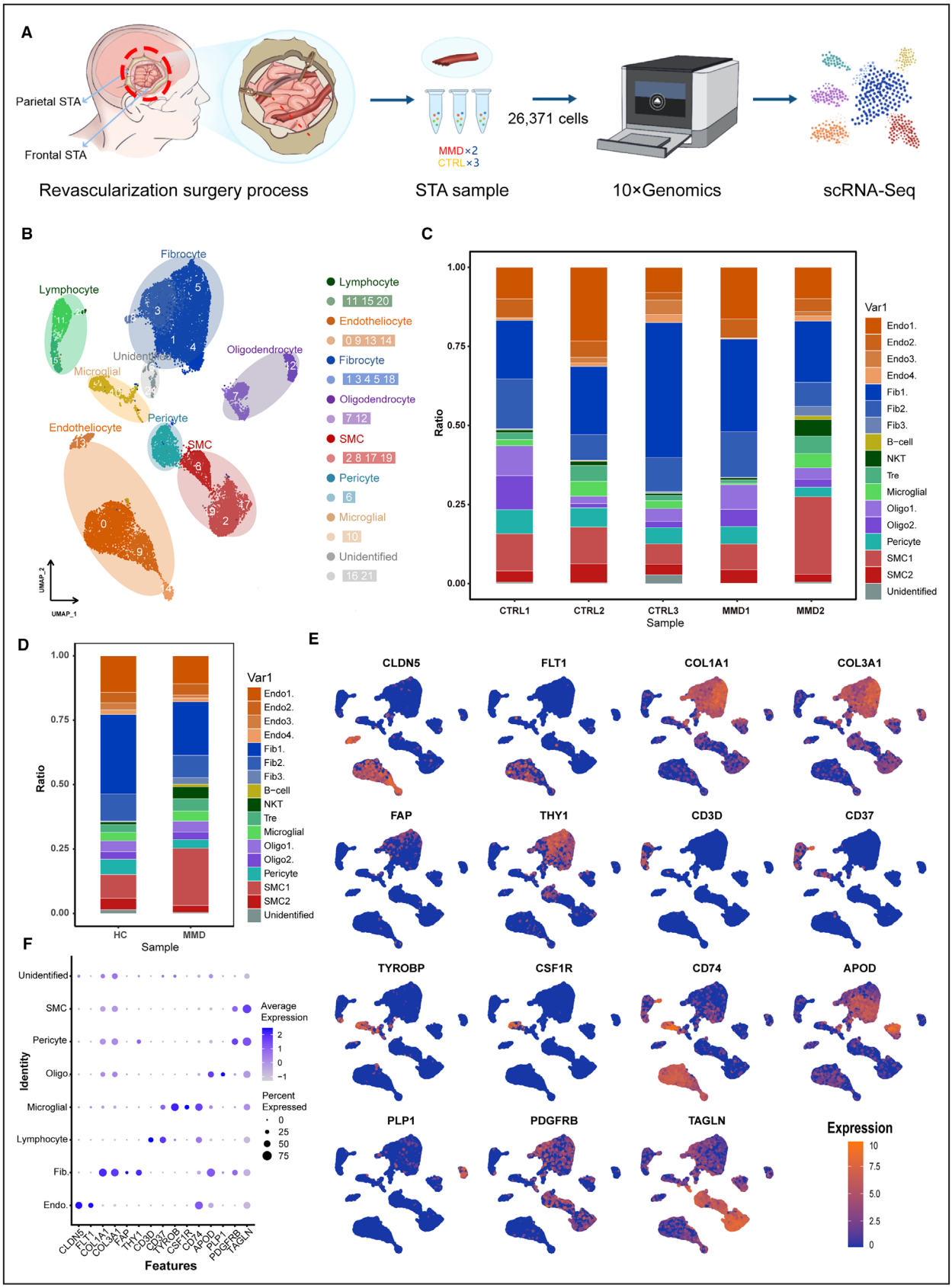
A
Parietal STA
Frontal STA
Revascularization surgery process
MMD×2
CTRL×3
STA sample
26,371 cells
10×Genomics
scRNA-Seq
B
Fibrocyte
Lymphocyte
Oligodendrocyte
Unidentified
Microglial
Pericyte
Endotheliocyte
SMC
UMAP_2
UMAP_1
Lymphocyte
11 15 20
Endotheliocyte
0 9 13 14
Fibrocyte
1 3 4 5 18
Oligodendrocyte
7 12
SMC
2 8 17 19
Pericyte
6
Microglial
10
Unidentified
16 21
C
Ratio
1.00
0.75
0.50
0.25
0.00
CTRL1
CTRL2
CTRL3
MMD1
MMD2
Sample
Var1
Endo1.
Endo2.
Endo3.
Endo4.
Fib1.
Fib2.
Fib3.
B−cell
NKT
Tre
Microglial
Oligo1.
Oligo2.
Pericyte
SMC1
SMC2
Unidentified
D
Ratio
HC
MMD
Sample
E
CLDN5
FLT1
COL1A1
COL3A1
FAP
THY1
CD3D
CD37
TYROBP
CSF1R
CD74
APOD
PLP1
PDGFRB
TAGLN
Expression
F
Identity
Unidentified
SMC
Pericyte
Oligo.
Microglial
Lymphocyte
Fib.
Endo.
Average Expression
Percent Expressed
Features

clusters displayed distinct gene expression profiles between MMD and HC samples. The SMC1 cluster highly expressed *C11orf96*, *XIST*, *BCAM*, *SNCG*, and *ACTA1*compared with HC, while the SMC2 cluster highly expressed *RPL36A*, *ACKR3*, *XIST*, *HIST1H4C*, and *RPS10* (Figure 2A and 2B; Figure S6A and S6B). Next, we conducted a further functional analysis of these 2 clusters of SMCs. There were significant differences in pathway expression between clusters of SMC1 and SMC2. The SMC1 cluster exhibited high expression of respiratory electron transport, citric acid cycle and respiratory electron transport, muscle contraction, and so on. (Figure 2C). While the SMC2 cluster exhibited high expression of signal recognition particle–dependent cotranslational protein targeting to membrane, eukaryotic translation termination,and so on (Figure S6C).

The ECs in the STA can be classified into 4 groups based on distinct gene expression profiles (Figure S7A). The Endo1 group highly expressed *ACKR1*, *SELE*, *LHX6*, *CSF3*, and *CCL23*; the Endo2 group highly expressed *BTNL9*, *SOX17*, *RBP7*, *SEMA3G*, and *CD300LG*; the Endo3 group highly expressed *TFF3*, *CCL21*, *PKHD1L1*, *NTS*, and *STAB2*; and the Endo4 group highly expressed *ITLN1*, *MPZL2*, *F5*, *IRF6*, and *AC004540.4* (Figure S7B). The pathway expression of the 4 EC types also exhibits significant differences (Figure S7C). The Endo1 cluster displayed distinct gene expression profiles between MMD and HC samples. Among them, *XIST*, *ABHD6*, *LFNG*, *BLOC1S1*, and *HRCT1* were significantly upregulated in MMD, while *AKAP12*, *STC1*, *FOSL1*, *CSF3*, and *SERPINE1* were significantly downregulated (Figure S7D and S7E).

Immune Cells and Their Interaction With Other Cell Types in Human STA Tissues

Through the analysis of immune cells in the STA samples, we found the distinct gene expression profiles between MMD and HC samples. *TRDV2*, *TRDC*, *TRGV9*, *SELL*, and *XCL2* genes were significantly upregulated in MMD, while *LMNA*, *FKBP5*, *CFD*, *RPS4Y1*, and *DDX3Y* genes were significantly downregulated (Figure 3A and 3B). The first 20 marker genes of the NKT type are shown in Table S2. Gene set enrichment analysis reveals the activation of cytoplasmic translation and adaptive immune responses of NKT cells in MMD, while several processes related to regulation of programmed cell death, gene expression regulation, and stress response were suppressed (Figure 3C). Cell–cell communication analysis revealed that the SMC1, Endo2, and Fib1 clusters were significantly associated with other cell clusters in the STA wall, indicating a key role of these 3 cell types in the vascular remodeling observed in MMD vasculature. We found the strong interactions between immune cells (NKT cells, regulatory T (Treg) cells, and B cells) and SMC clusters (SMC1 and SMC2), EC clusters (Endo1, Endo2, Endo3, and Endo4), and fibrocyte clusters (Fib1, Fib2 and Fib3) (Figure 3D). Figure 3E shows the interaction network mediated by the macrophage migration inhibitory factor (MIF) signaling pathway between different cell types. We identified extensive interactions between immune cells and other cell types. Immune cells play a significant role in the MIF signaling pathway, especially as the influencer. SMCs also play a prominent role as both senders and influencers in MIF signaling (Figure 3F). Immune cells, including B cells, NKT cells, and Treg cells, can act as signal sources, transmitting signals to various target cell types, such as SMCs and ECs (Figure 3G). To further characterize the functional heterogeneity of NKT cells, we performed subclustering on NKT cells. This analysis revealed transcriptionally distinct subpopulations, including *NKT1* (organization-resident NKT, *trNKT*), *NKT3* (mixed-type NKT, γδ-*NKT*) *NKT2* (vytotoxic NKT), *NKT4* (activated NK-like NKT), *NKT5* (migratory NKT) and *NKT6* (perivascular NKT) enriched in MMD samples (Figure S8). Gene ontology analysis results revealed the functional pathways enriched in *NKT1* through *NKT6* (Figures S9 through S11). These results suggest that the interactions between immune cells and the constituent cells of the STA wall may be closely associated with the pathological changes of vessels in MMD.

Colocalization of CD74 with CD44 or CXCR4 in ECs of MMD Promotes EC Proliferation and Angiogenesis

We further analyzed the expression patterns of MIF and its primary receptors across different cell types. The results showed that MIF was highly expressed in all cell types. ACKR3 was mainly highly expressed in SMCs and fibroblasts, CD74 was predominantly expressed in ECs and immune cells, CXCR4 was mainly expressed in immune cells, and CD44 was mainly highly expressed in both immune cells and SMCs (Figure 4A). Subsequently, we cocultured human brain microvascular endothelial cells (HBMECs) with serum from patients with MMD and HCs, respectively. Compared with the HC group, HBMEC cells stimulated with MMD serum showed a significant increase in the expression levels of MIF, CD74, CD44, and CXCR4 (Figure 4B through 4D). Additionally, colocalization of CD74 with CD44, and CD74 with CXCR4 was increased in HBMEC cells stimulated with MMD serum (Figure 4B through 4E). These results showed that MMD serum can enhance the colocalization of CD74 with CD44 or CXCR4 in HBMEC cells. We also analyzed the ligand receptor–mediated signaling interactions between immune cells and other cell types. Immune cells, including NKT, Treg, and B cells, interact with other cell types through pathways such as

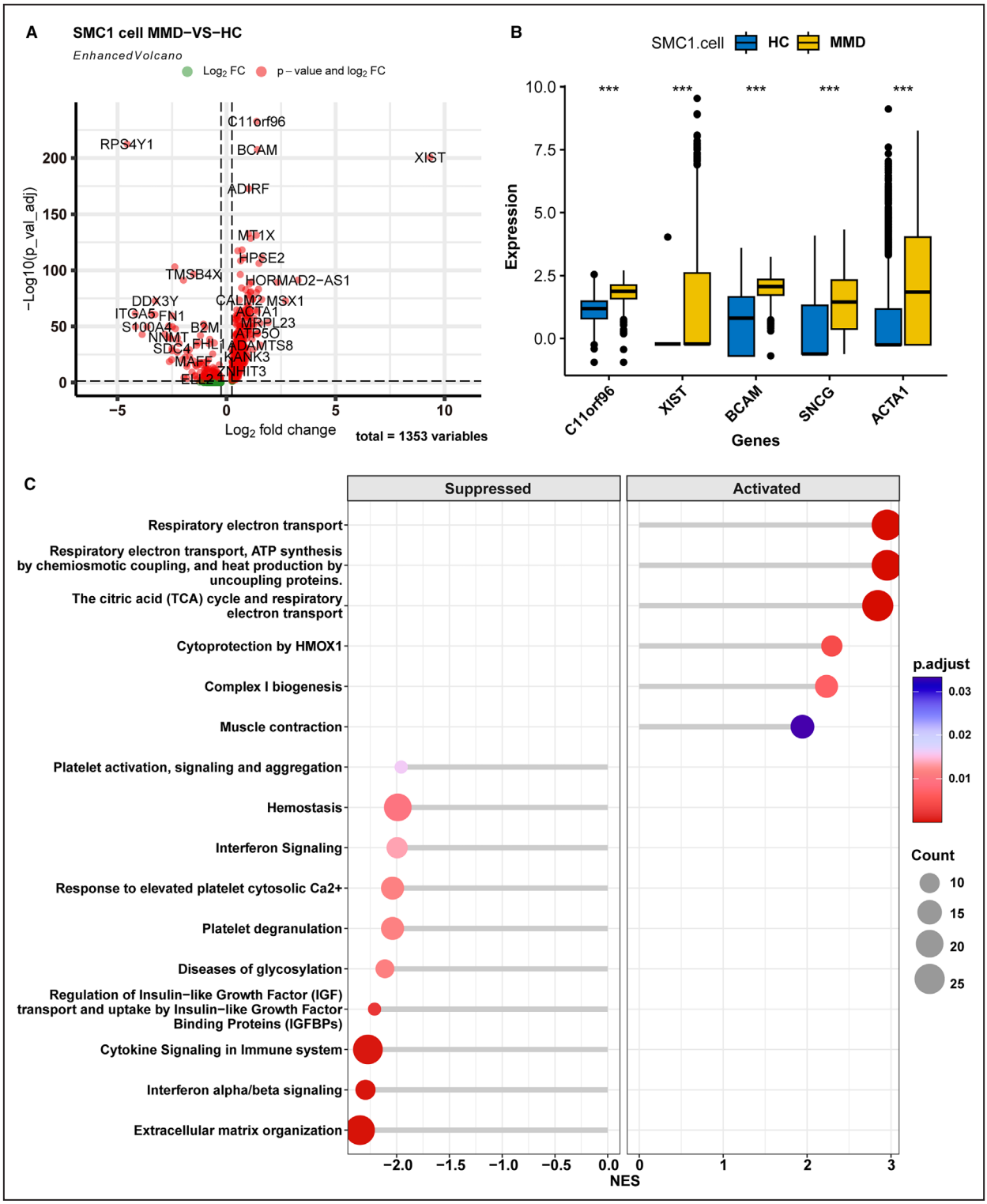

Figure 2. Heterogeneity of SMC1 group in human STA tissues between MMD and HC.
A, Volcano plot showing the genes differentially expressed in SMC1 cells between MMD and HC. Red dots represent significantly differentially expressed genes, with key genes labeled. **B**, Box plots depicting the expression levels of selected genes (*C11orf96, XIST, BCAM, SNCG*, and *ACTA1*) in SMC1 cells for patients with MMD and HCs, with significant differences indicated (***P<0.001). **C**, Dot plot showing gene set enrichment analysis of biological pathways in SMC1 cells. Pathways on the left are suppressed, while those on the right are activated in patients with MMD compared with HCs. P values calculated by means of Wilcox test. ***P<0.001. HC indicates healthy control; MMD, moyamoya disease; SMC, smooth-muscle cell; and STA, superficial temporal artery.

MIF-ACKR4, MIF-(CD74+CXCR4), MIF-(CD74+CD44) and C-C motif chemokine ligand-5-ACKR1 (Figure 4F). To study the effects of CD74 and CD44 coexpression, as well as CD74 and CXCR4 coexpression on HBMEC cells, we transfected HBMEC cells with small interfering RNA plasmids to simultaneously knock down the expression of CD74 and CD44, and CD74 and CXCR4. 5-Ethynyl-2′-deoxyuridine results showed that the proliferation capacity of HBMEC cells were significantly decreased following the simultaneous knockdown of CD74 and CD44, as well as CD74 and CXCR4 (Figure 5A through 5C). We also assessed the tube formation ability of HBMEC cells following the simultaneous knockdown. The results showed that both the number of branches and total length of tube formations in HBMEC cells were significantly decreased following the co-knockdown (Figure 5D-5F). These results indicate that co-knockdown of CD74 and CD44, as well as CD74 and CXCR4 can significantly reduce the proliferation and angiogenesis capacity of HBMEC cells.

Human Brain VSMCs and HBMECs Exhibited Enhanced Proliferation and Adhesion Abilities, and Cytoskeletal Enlargement in Coculture With NKT Cells in the Presence of MMD Serum

Through the analysis of interactions between immune cells and other cell types, we found that NK cells exhibited extensive cellular communication with other cell types, particularly SMCs, ECs, and fibroblasts (Figure 5G). We also performed immunohistochemistry staining on the STA of patients with MMD and HCs to examine the NKT invasion in the biopsies of MMD. The results demonstrated the infiltration of NKT cells (CD56+) in the STA of patients with MMD, compared with the HC group (Figure 6). Subsequently, we further investigated the effects of immune cells, including NKT and Treg cells, on SMCs and ECs. We first treated human brain vascular smooth-muscle cells (HBVSMCs) with serum from patients with MMD and HCs, respectively, and then cocultured the treated HBVSMCs with NK cells (Figure 5H). Compared with HBVSMCs treated with HC serum, MMD serum-treated HBVSMCs with NKT cell coculture exhibited an upregulation of vinculin and F-action, indicating an enhanced cell adhesion and an enlarged cytoskeleton (Figure 5I). Flow cytometry cell cycle analysis showed that in the presence of NKT cells, the HBMECs treated with MMD serum exhibited a higher proportion of cells in the S phase compared with HBVSMCs treated with HC serum, indicating an enhanced proliferative capacity in MMD serum-treated HBVSMCs (Figure 7C and 7D).We also applied the same approach to establish a coculture system of NKT cells and HBMECs and found that in the presence of NKT cells, HBMECs also exhibited enhanced adhesion and an enlarged cytoskeleton following MMD serum treatment (Figure 7A). Additionally, after coculturing HBMECs treated with MMD serum with NKT cells, the proliferation capacity of NKT cells was significantly enhanced (Figure 7B). Tube formation assays revealed that in the NKT–HBMEC coculture system, HBMECs treated with MMD serum exhibited a greater angiogenesis capacity (Figure 7E and 7G). Meanwhile, MMD serum-treated HBMECs exhibited a higher proportion of cells in the S phase and an increased cell proliferation rate (Figure 7F and 7G). These results revealed that MMD serum can promote the proliferation of NKT and Treg cells, and in the presence of these 2 cells, MMD serum can enhance the proliferation, adhesion capacity, and cytoskeletal enlargement of the cocultured HBVSMCs. MMD serum can also enhance the proliferation, adhesion capacity, cytoskeletal enlargement, and angiogenesis ability of the cocultured HBMECs.

To verify the consistency of gene expression levels in NKT cells both in vitro and in vivo, a coculture system of HBMECs and NKT cells was established. Compared with the control group, there was no significant difference in the expression levels of HLA-B, RPS10, and RPS4Y1 proteins and mRNA in NKT cells of the HC group (Figure S12A through S12D). Compared with the HC group, the expression levels of HLA-B and RPS10 proteins and mRNA in NKT cells of the MMD group significantly increased, while the expression levels of RPS4Y1 protein and mRNA significantly decreased (Figure S12E through S12G).

Integrated Analysis of RNA Sequencing and sc-RNAseq of STA Samples Identified Key Genes Associated With the Pathogenesis of MMD

At the same time, we performed RNA sequencing on 13 STA samples including 10 samples from patients with

Figure 3. Immune cells and their interaction with other cell types in human STA tissues.
A, Violin plots of differentially expressed genes between patients with MMD and HCs in NKT cells. **B**, Volcano plot comparing gene expression between patients with MMD and HCs in NKT cells. **C**, Bar plot showing enriched biological pathways in the clusters of NKT cells. **D**, Chord diagram showing the interactions between different cell types mediated by MIF signaling. **E**, Heatmap showing the functional roles of different cell types in the MIF signaling pathway, including their roles as signal senders, receivers, mediators or influencers. **F**, Source–target interaction map showing the transmission pathways of MIF signaling between different cell types. **G**, Source-target interaction map of MIF signaling between immune cells and vascular wall cells, specifically illustrating how immune cells (B cells, NKT cells, Treg cells) transmit MIF-related signals to SMCs and ECs, highlighting immune–vascular crosstalk that contributes to pathological remodeling in MMD. EC indicates endothelial cell; GOBP, gene ontology biological process; HC, healthy control; MIF, migration inhibitory factor; MMD, moyamoya disease; NKT, natural killer T; SMC, smooth-muscle cell; STA, superficial temporal artery; and Treg, regulatory T cells.

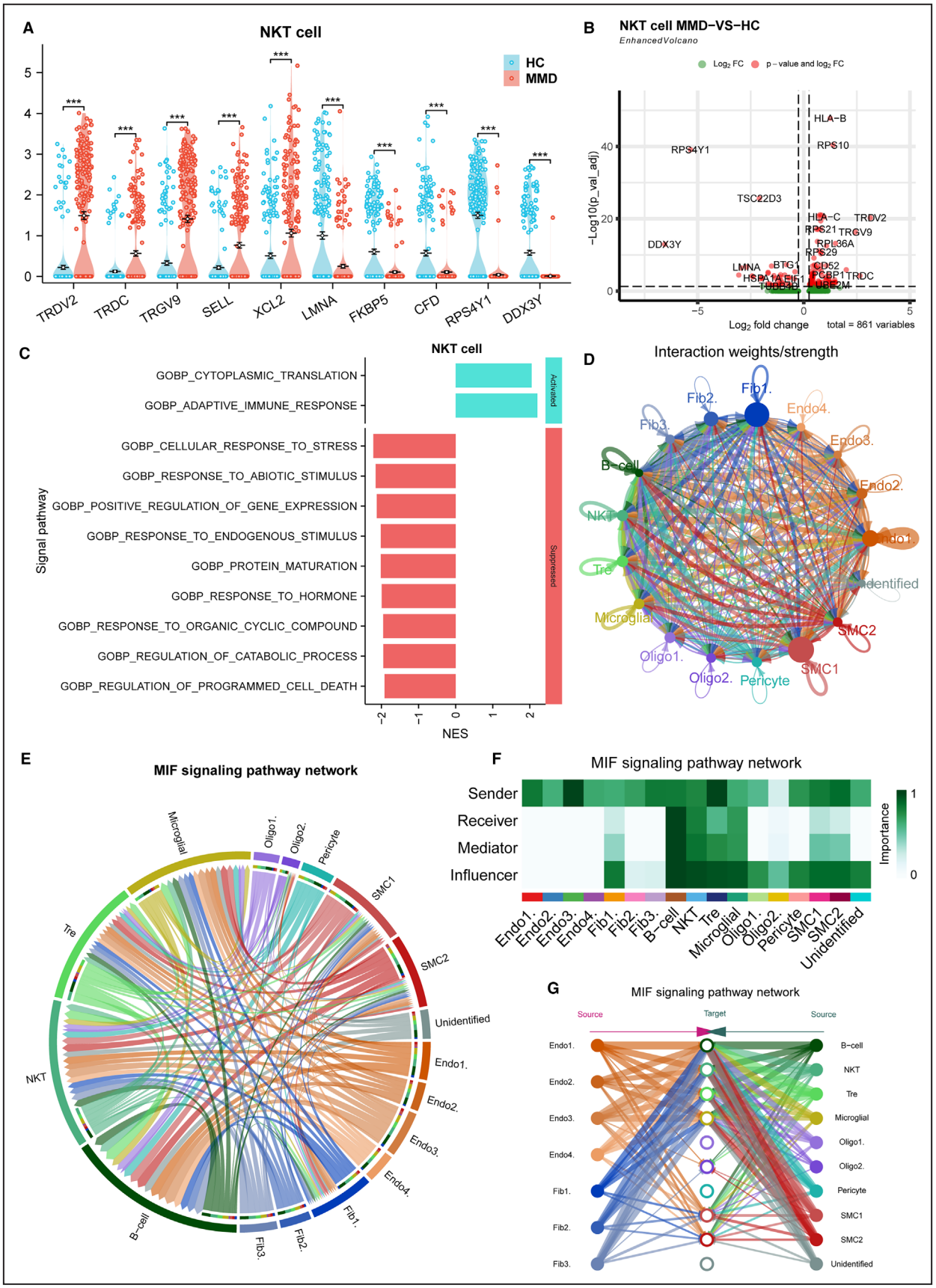
A
NKT cell
HC
MMD
TRDV2
TRDC
TRGV9
SELL
XCL2
LMNA
FKBP5
CFD
RPS4Y1
DDX3Y
B
NKT cell MMD−VS−HC
EnhancedVolcano
Log2 FC
p − value and log2 FC
HLA−B
RPS10
RPS4Y1
TSC22D3
HLA−C
TRDV2
RPS21
TRGV9
DDX3Y
RPL36A
RPS29
LMNA
BTG1
CD52
PCBP1
TRDC
−Log10(p_val_adj)
Log2 fold change
total = 861 variables
C
NKT cell
GOBP_CYTOPLASMIC_TRANSLATION
GOBP_ADAPTIVE_IMMUNE_RESPONSE
GOBP_CELLULAR_RESPONSE_TO_STRESS
GOBP_RESPONSE_TO_ABIOTIC_STIMULUS
GOBP_POSITIVE_REGULATION_OF_GENE_EXPRESSION
GOBP_RESPONSE_TO_ENDOGENOUS_STIMULUS
GOBP_PROTEIN_MATURATION
GOBP_RESPONSE_TO_HORMONE
GOBP_RESPONSE_TO_ORGANIC_CYCLIC_COMPOUND
GOBP_REGULATION_OF_CATABOLIC_PROCESS
GOBP_REGULATION_OF_PROGRAMMED_CELL_DEATH
Activated
Suppressed
Signal pathway
NES
D
Interaction weights/strength
Fib1.
Fib2.
Fib3.
Endo4.
Endo3.
B−cell
Endo2.
NKT
Endo1.
Tre
Unidentified
Microglial
SMC2
Oligo1.
SMC1
Oligo2.
Pericyte
E
MIF signaling pathway network
Microglial
Oligo1.
Oligo2.
Pericyte
SMC1
SMC2
Unidentified
Endo1.
Endo2.
Endo3.
Endo4.
Fib1.
Fib2.
Fib3.
B−cell
NKT
Tre
F
MIF signaling pathway network
Sender
Receiver
Mediator
Influencer
Importance
Endo1.
Endo2.
Endo3.
Endo4.
Fib1.
Fib2.
Fib3.
B−cell
NKT
Tre
Microglial
Oligo1.
Oligo2.
Pericyte
SMC1
SMC2
Unidentified
G
MIF signaling pathway network
Source
Target
Source
Endo1.
Endo2.
Endo3.
Endo4.
Fib1.
Fib2.
Fib3.
B−cell
NKT
Tre
Microglial
Oligo1.
Oligo2.
Pericyte
SMC1
SMC2
Unidentified

MMD and 3 samples from HCs (Figure 8A). DEG analysis between the MMD and HC groups was performed using the DESeq2 R package, extracting genes with log2FoldChange >1 and adjusted $P<0.05$. Finally, 2547 DEGs were extracted (Figure 8B). Then, we further conducted an integrative analysis of the RNA sequencing data with the sc-RNAseq data from the STA samples. We then used the weighted correlation network analysis R package to select gene sets with a Pearson correlation coefficient >0.7 and a P value <0.01 from the 2547 DEGs, and subsequently constructed a gene clustering dendrogram (Figure 8C). Next, we extracted the top 5 DEGs from each cell subpopulation in the MMD and HC groups from the sc-RNAseq data, resulting in a total of 82 genes. We then intersected these 82 genes with the 2547 DEGs from RNA sequencing, ultimately identifying 12 overlapping genes (Figure 8D and 8J).

When the soft threshold reached 11, the fit index (R^2) exceeded 0.8, indicating that the network exhibited scale-free topology while maintaining a reasonable average connectivity. This made it suitable for subsequent weighted correlation network analysis, and we therefore set 11 as the optimal power value (Figure 8E). The Eblue and Turquoise gene modules were significantly positively correlated with MMD group and negatively correlated with HC group, suggesting that these gene modules may play a key role in the molecular mechanisms of MMD (Figure 8F). Weighted correlation network analysis revealed that a large number of DEGs were significantly associated with MMD (Figure 8G). We then constructed a protein–protein interaction network using STRING (https://string-db.org/) and identified 5 key genes through the Degree algorithm including *CFD*, *GPX3*, *SERPINE1*, *SELE*, and *SLC40A1* (Figure 8H). Subsequently, we further predicted the top 10 drugs on the basis of their target binding scores. Figure 8I showed the potential associations between the 5 key genes in the turquoise module and various drugs. Notably, formaldehyde, metformin, and rifaximin showed significant associations with these genes.

DISCUSSION

MMD is a chronic cerebrovascular disorder characterized by the progressive occlusion of pathological arteries, which may lead to severe ischemic or hemorrhagic stroke. To date, there is a lack of systematic analysis on the cellular composition and gene expression profiles of diseased arteries in MMD, which has limited the understanding of the underlying mechanisms driving its pathological changes. The present study first comprehensively revealed the cellular composition and immune infiltration of the superficial temporal artery in MMD. A total of 21 cell subpopulations were identified and further clarified into 7 major cell groups, including ECs, SMCs, fibroblasts, and others. We observed an abnormal increase in the proportion of SMCs in the STA of MMD and identified distinct gene expression profiles of SMCs between patients with MMD and HCs. Additionally, through in vitro experiments, we found that NKT and Treg immune cells from MMD patients promote the proliferation, migration, adhesion, and cytoskeletal enlargement of ECs and SMCs. Finally, through integrative analysis of sc-RNAseq and RNA sequencing data, we identified potential key hub genes involved in the pathogenesis of MMD. This study provides new insights into understanding vascular pathology and exploring the underlying pathogenesis in MMD.

Previous histological studies of pathological arteries in MMD revealed that the primary pathological changes include concentric intimal thickening, abnormal abundance of SMC in the intima, and disruption of the internal elastic lamina.[3,4,18,19] These pathological alterations suggest excessive proliferation of SMCs and ECs in the arterial walls of MMD. Moreover, the abnormal accumulation of SMCs in the intima, which are normally confined to the media, suggests the potential migration of SMCs from the media to the intima.[20] However, the underlying causes of these vascular lesions remain unknown. Currently, numerous omics-based sequencing studies on intracranial arteries of MMD have uncovered several potential gene targets associated with the pathogenesis of MMD. A recent study conducted RNA sequencing on the STA of patients with MMD and identified the downregulation of *DSG2*. Reduction of this gene promoted proliferation and migration of ECs and led to impaired angiogenesis.[21] Another study analyzed the RNA sequencing data from the middle cerebral artery of patients with MMD and highlighted that extracellular matrix and mitochondrial function are central molecular mechanisms in MMD and revealed

Figure 4. Colocalization of CD74 with CD44 or CXCR4 was observed in endothelial cells of MMD.
A, Violin plots showing the expression distribution of MIF and its receptors (ACKR3, CD74, CXCR4, CD44) in different cell types. **B**, Immunofluorescence showing the colocalization of CD74 with CD44 in HBMEC cells. Bar=50μm, CD44 (green), CD74 (red), DAPI (blue). **C**, Western blot analysis detecting the MIF, CD74, CD44, CXCR4, and β-actin expression in HBMEC cells, along with colocalization of CD74 with CD44 or CXCR4. **D**, Immunofluorescence showing the colocalization of CD74 with CXCR4 in HBMEC cells. Bar=50μm, CD44 (green), CD74 (red), DAPI (blue). **E**, Flow cytometry analysis detecting the CD74 and CD44 or CXCR4 colocalization in HBMEC cells. **F**, Ligand-receptor interaction network displaying communication probabilities between different cell types. HBMEC indicates human brain microvascular endothelial cell; HC, healthy control; MIF, migration inhibitory factor; MMD, moyamoya disease; NKT, natural killer T; TGFB1, transforming growth factor B1; TNF, tumor necrosis factor; VEGFB, vascular endothelial growth factor B; and VEGFR1, vascular endothelial growth factor receptor 1.

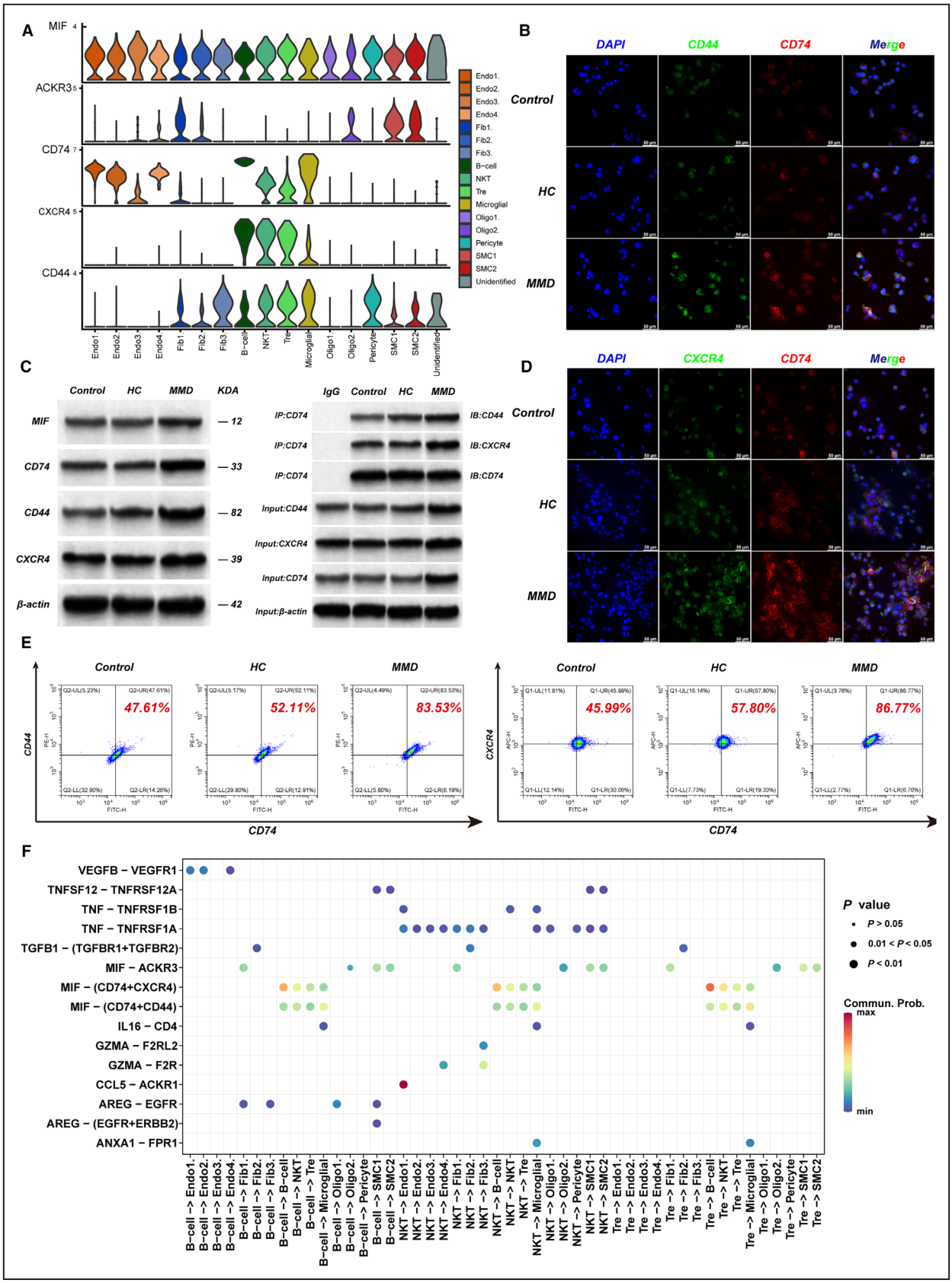
A
MIF
ACKR3
CD74
CXCR4
CD44
Endo1.
Endo2.
Endo3.
Endo4.
Fib1.
Fib2.
Fib3.
B−cell
NKT
Tre
Microglial
Oligo1.
Oligo2.
Pericyte
SMC1
SMC2
Unidentified
B
DAPI
CD44
CD74
Merge
Control
HC
MMD
C
Control
HC
MMD
KDA
MIF
CD74
CD44
CXCR4
β-actin
12
33
82
39
42
IgG
IP:CD74
IB:CD44
IB:CXCR4
IB:CD74
Input:CD44
Input:CXCR4
Input:CD74
Input:β-actin
D
DAPI
CXCR4
CD74
Merge
E
Control
HC
MMD
CD44
CD74
47.61%
52.11%
83.53%
CXCR4
45.99%
57.80%
86.77%
F
VEGFB − VEGFR1
TNFSF12 − TNFRSF12A
TNF − TNFRSF1B
TNF − TNFRSF1A
TGFB1 − (TGFBR1+TGFBR2)
MIF − ACKR3
MIF − (CD74+CXCR4)
MIF − (CD74+CD44)
IL16 − CD4
GZMA − F2RL2
GZMA − F2R
CCL5 − ACKR1
AREG − EGFR
AREG − (EGFR+ERBB2)
ANXA1 − FPR1
P value
P > 0.05
0.01 < P < 0.05
P < 0.01
Commun. Prob.
max
min

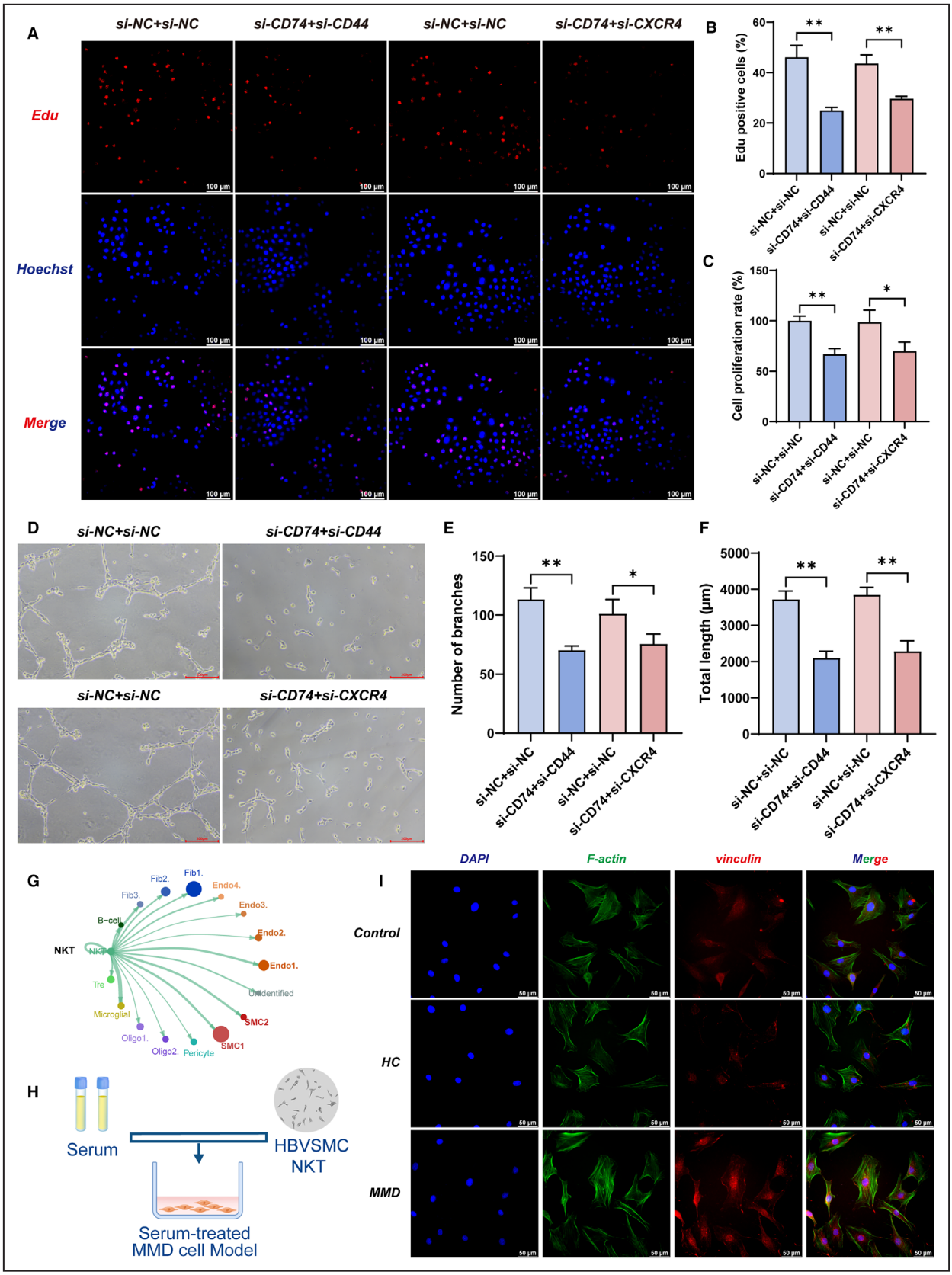
A
si-NC+si-NC
si-CD74+si-CD44
si-NC+si-NC
si-CD74+si-CXCR4
Edu
Hoechst
Merge
100 μm
B
Edu positive cells (%)
60
40
20
0
**
**
si-NC+si-NC
si-CD74+si-CD44
si-NC+si-NC
si-CD74+si-CXCR4
C
Cell proliferation rate (%)
150
100
50
0
**
*
si-NC+si-NC
si-CD74+si-CD44
si-NC+si-NC
si-CD74+si-CXCR4
D
si-NC+si-NC
si-CD74+si-CD44
si-NC+si-NC
si-CD74+si-CXCR4
E
Number of branches
150
100
50
0
**
*
si-NC+si-NC
si-CD74+si-CD44
si-NC+si-NC
si-CD74+si-CXCR4
F
Total length (μm)
5000
4000
3000
2000
1000
0
**
**
si-NC+si-NC
si-CD74+si-CD44
si-NC+si-NC
si-CD74+si-CXCR4
G
Fib1.
Fib2.
Fib3.
Endo4.
Endo3.
B-cell
Endo2.
NKT
NK1
Endo1.
Tre
Unidentified
Microglial
SMC2
Oligo1.
SMC1
Oligo2.
Pericyte
H
Serum
HBVSMC
NKT
Serum-treated
MMD cell Model
I
DAPI
F-actin
vinculin
Merge
Control
HC
MMD
50 μm

Figure 5. Colocalization of CD74 with CD44 or CXCR4 promotes the proliferation and angiogenesis of endothelial cells in MMD.

A, Edu assay assessing the proliferative capacity of HBMEC cells after simultaneous knockdown of CD74 and CD44 or CXCR4. Bar = 100 μm. **B** and **C**, Bar chart displaying the Edu positive cells and cell proliferation rate of HBMECs. *P<0.05, **P<0.01. **D**, Tube formation assay assessing the angiogenesis capacity of HBMECs after simultaneous knockdown of CD74 and CD44 or CXCR4. Bar=200 μm. **E** and **F**, Bar chart displaying the number of branches and total length of HBMECs. *P<0.05, **P<0.01. **G**, Network diagram illustrating the interactions of NKT cell with other cell types. **H**, Schematic diagram showing the co-culture system of NKT cells and HBVSMCs. **I**, Immunofluorescence assay assessing the expression levels of vinculin and F-actin in HBVSMCs after coculture with NKT cells. Bar=50 μm, F-actin (green), Vinculin (red), DAPI (blue). *P* values calculated by means of Student's *t* test, 1-way ANOVA, and Tukey's test. **P<0.01. Edu indicates 5-Ethynyl-2′-deoxyuridine; HBMEC, human brain microvascular endothelial cell; HBVSMC, human brain vascular smooth-muscle cell; HC, healthy control; MMD, moyamoya disease; and NKT, natural killer T.

sex-specific differences in gene expression within the intracranial arteries.[22] Currently, the most extensively studied gene in the field of MMD is *RNF213*..[23,24] A recent study performed whole-genome sequencing on STA specimens and identified mutation types of *RNF213* in patients with MMD. They found that reduced *RNF213* expression led to increased EC proliferation, migration, and tube formation through activation of the Hippo pathway.[25] Although previous studies have identified some potential targets, sequencing on the entire vascular tissue cannot reflect the specific roles that individual cell types within the vessel wall play in MMD, as the vessel wall is composed of multiple cell types. This limitation hinders the investigation of the mechanisms by which specific cell types contribute to the pathogenesis of MMD.

sc-RNAseq is a novel technique that allows for the genetic profiling of biological samples at the resolution of individual cells.[9] At present, important applications of sc-RNAseq technology have been used in the research field of MMD. Tang et al[17] first found the single-cell sequencing landscape of peripheral blood in MMD through sc-RNAseq of peripheral blood from patients with MMD, revealing cellular and gene expression heterogeneity. They identified key genes related to MMD, such as *PTP4A1*, *SPINT2*, and *CSTB*, and revealed the differentiation of immune cells and the relationship between immune cells in MMD. Ge et al[26] also used sc-RNAseq for peripheral blood from MMD patients to identify immune dysfunction in MMD, characterized primarily by disturbances in T-cell subpopulations, including a reduction in effector T cells and an increase in Tregs. Both studies identified alterations of immune cells in MMD. However, previous studies have focused solely on peripheral blood, and to date, no single-cell sequencing has been conducted on MMD-affected vessels. This results in a lack of direct evidence for studying the cellular composition and functional changes in diseased arteries. Here, we performed the first sc-RNAseq study on the STA of MMD patients. We observed a significant increase in the proportion of SMCs in MMD arteries, corroborating the previously reported histological findings of excessive SMC proliferation.[3,4,18,19] Additionally, we classified the SMCs in the STA into 2 groups, with SMC1 being upregulated in patients with MMD compared with HCs, while SMC2 was downregulated. We found that *MRPL23* was significantly upregulated in SMC1 of MMD. *MRPL23* has been reported to promote cancer cell metastasis and facilitate epithelial–mesenchymal transition in lung metastasis.[27] This suggests that the overexpression of this gene in the SMC1 subpopulation of MMD may contribute to the promotion of SMC migration.

An increasing number of studies have demonstrated that immune responses may play a crucial role in the pathogenesis of MMD.[28–30] Through the analysis of immune cells in STA samples, we found an increased amount of NKT cells and identified significant changes in the gene expression profile of NKT cells in STA samples from patients with MMD. We found that *SLC2* and *SELL* expression was significantly upregulated in NKT cells of MMD. Selectin L is a critical cell adhesion molecule involved in leukocyte trafficking, particularly in guiding lymphocytes to secondary lymphoid organs and sites of inflammation.[31] Peng et al[32] demonstrated that under viral infection or pathological conditions, *SELL* can regulates the migration of NKT cells to pathological sites and promotes their proliferation and effector functions. Solute carrier family 2 is a family of membrane transport proteins that primarily mediate the uptake of glucose into cells and plays a crucial role in cellular metabolism, especially in tissues like the brain, liver, and muscles.[33,34] In several rapidly growing cells, such as solid tumor cells, the overexpression of *SLC2* can promote glucose uptake and energy production, thereby facilitating functions such as cell proliferation and migration.[35,36] *FKBP5* encoding a molecular chaperone, which was widely involved in the regulation of various cellular signaling pathways, affecting processes such as cell proliferation, survival, and antiapoptosis.[37] Liu et al[38] found that in pancreatic β cells, the downregulation of *FKBP5* improved cell survival and function by regulating the protein kinase B/forkhead box O1 signaling pathway, thereby enhancing the proliferative capacity of β cells in an inflammatory environment. The changes of these gene expressions could promote proliferation and migration of NK cells,

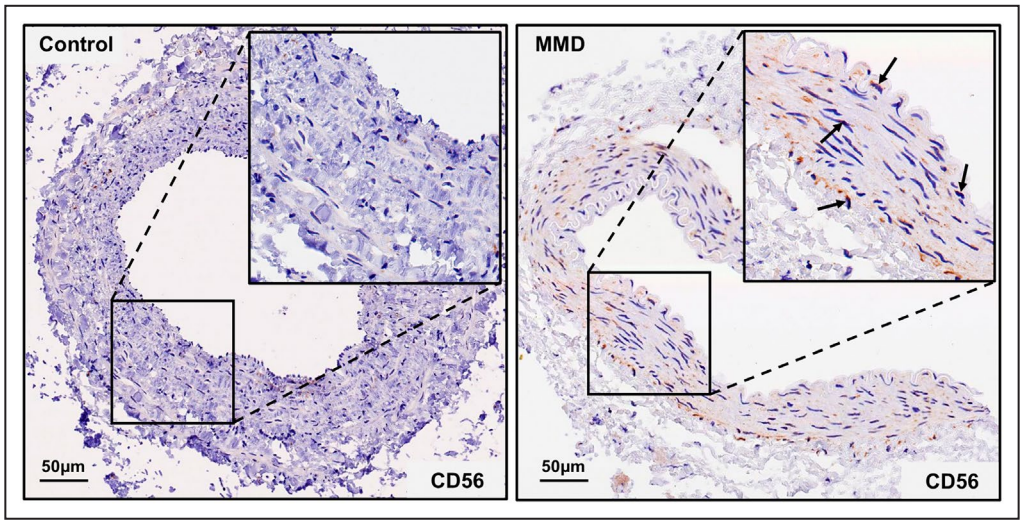

Figure 6. Representative immunohistochemistry images for CD56+ NKT cells in STA tissues.
Representative immunohistochemistry images for CD56 in STA samples from HCs and patients MMD. Positive CD56 staining, indicative of NKT cell infiltration, is observed in the MMD group (arrows), while it is absent in the HC group. Insets highlight the regions of interest, with magnification emphasizing the NKT cell localization in the vessel wall of the MMD sample. Scale bar=50 μm. HC, healthy control; MMD, moyamoya disease; NKT, natural killer T; and STA, superficial temporal artery

suggesting that in the STA of MMD, NK cells may be in an activated and enhanced state.

We also analyzed the immune cells within the STA wall and their interactions with other vascular wall component cells. NK cells were initially shown to have antiangiogenic functions, but recent evidence suggests that NK cells can play a pro-angiogenic role in humans.[39,40] Previous studies have found that NK cells can participate in regulating decidual vascular growth during pregnancy or promoting the formation of tumor vasculature by secreting angiogenic factors such as vascular endothelial growth factor, placental growth factor, and interleukin-8.[41,42] Throughout the process of angiogenesis, activated trophoblasts can directly or indirectly influence endothelial cells by activating the proangiogenic activity of NK cells.[43] Li et al[44] found that in pulmonary arterial hypertension, NK cells can interact with SMCs and ECs through C-C motif chemokine ligand-5, potentially promoting the proliferation of ECs and SMCs, thereby contributing to vascular remodeling. In conjunction with in vitro experiments, we found that under the presence of MMD serum, NKT cells can promote cytoskeletal enlargement in ECs and SMCs, enhancing their migratory and proliferative capacities, as well as promoting angiogenesis in ECs. Previous studies confirmed that the enlargement of the EC cytoskeleton and enhanced proliferative capacity may be potential causes of intimal thickening in MMD.[8] Other studies have also identified excessive proliferation and phenotypic changes in SMCs in MMD.[45,46] Therefore, previous studies and our findings suggest that NKT cells may influence ECs and SMCs through certain immune mechanisms, thereby contributing to the pathogenesis of MMD. However, the specific mechanisms or molecular pathways through which NK cells exert their effects on ECs and SMCs remain to be further investigated.

Limitations of the Study

This study also has some limitations. Analysis of tissues closer to the affected areas, such as the internal

Figure 7. HBVSMCs and HBMECs exhibited enhanced proliferation and adhesion abilities, and cytoskeletal enlargement in coculture with NKT cells in the presence of MMD serum.
A, Immunofluorescence assay assessing the expression levels of vinculin and F-actin in HBMECs after coculture with NKT cells. Bar=50 μm, F-actin (green), Vinculin (red), DAPI (blue). **B**, Flow cytometry analysis assessing the proliferative capacity of NKT cells cocultured with HBMECs. Bar chart displaying the counts of proliferated HBMECs. ***P*<0.01. **C**, Flow cytometry analysis assessing the cell cycle of HBVSMCs cocultured with NKT cells. **D**, Bar chart displaying the cell proliferation rate and relative cell cycle phase of HBMECs. ***P*<0.01. **E**, Tube formation assay assessing the angiogenesis capacity of HBMECs cocultured with NKT cells. Bar=200 μm. **F**, Flow cytometry analysis assessing the cell cycle of HBMECs cocultured with NKT cells. **G**, Bar chart displaying the cell proliferation rate, number of branched, total length, and relative cell cycle phase of HBMECs. **P*<0.05, ***P*<0.01. HBMEC indicates human brain microvascular endothelial cell; HBVSMC, human brain vascular smooth-muscle cell; HC, healthy control; MMD, moyamoya disease; and NKT, natural killer T.

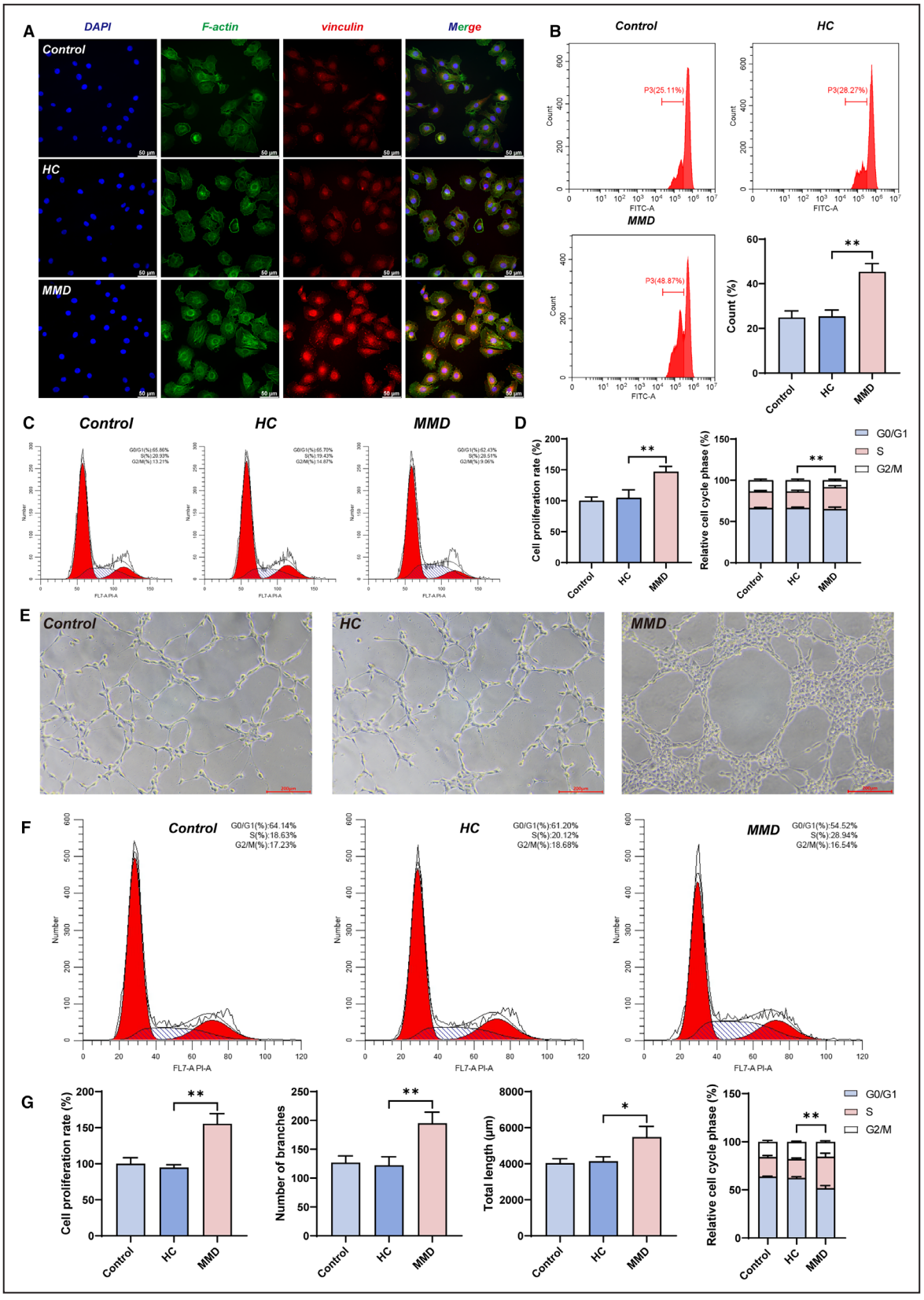

carotid artery or the middle cerebral artery, may provide deeper insights into the vascular pathology of MMD. In addition, the small cohort sample size resulted in a moderate sex imbalance between the MMD group and the control group, which might introduce residual confusion in our analysis. Due to the lack of animal models

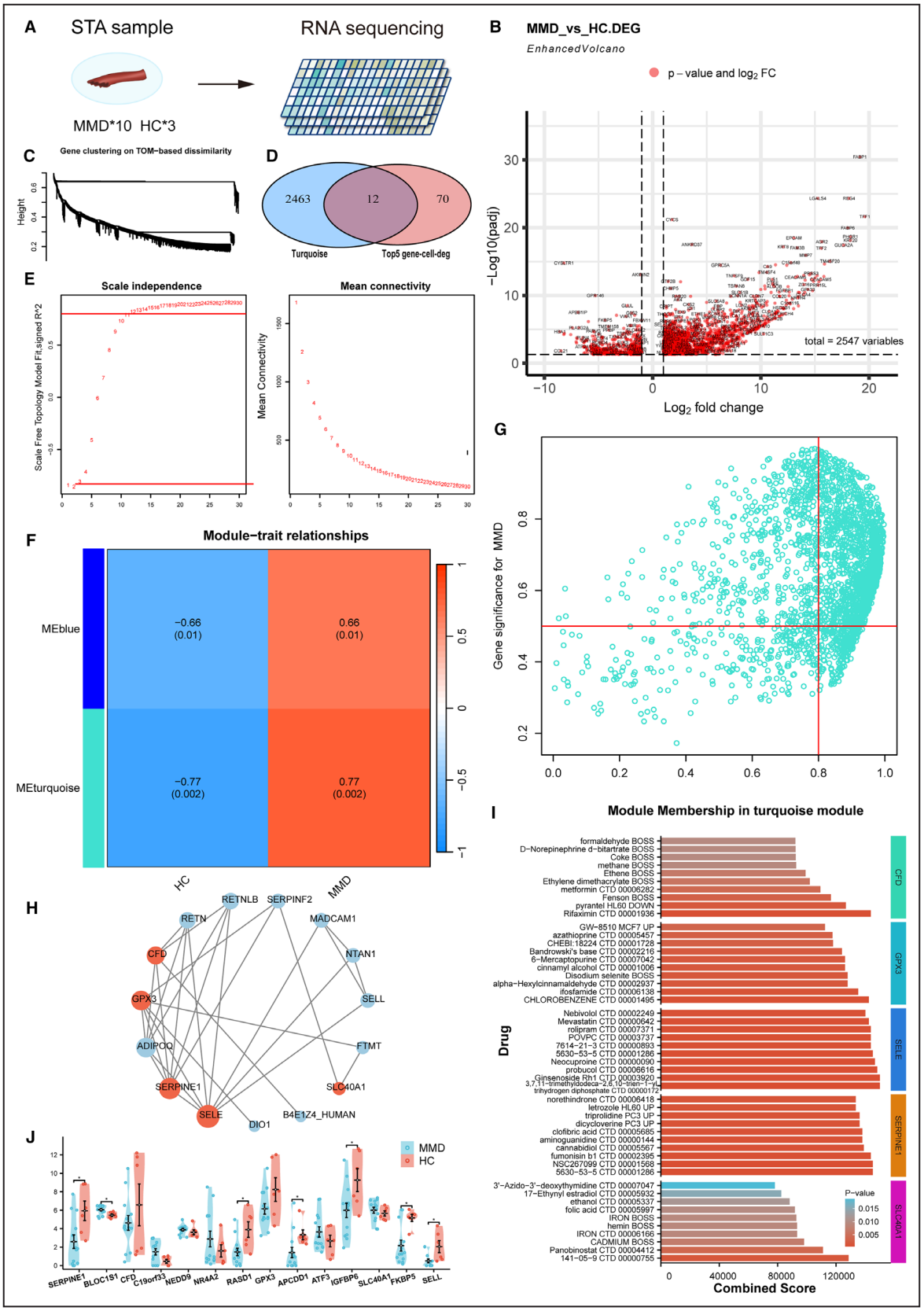
A
STA sample
RNA sequencing
MMD*10 HC*3
B
MMD_vs_HC.DEG
EnhancedVolcano
p – value and log2 FC
−Log10(padj)
Log2 fold change
total = 2547 variables
C
Gene clustering on TOM−based dissimilarity
Height
D
2463
12
70
Turquoise
Top5 gene-cell-deg
E
Scale independence
Scale Free Topology Model Fit,signed R^2
Mean connectivity
Mean Connectivity
F
Module−trait relationships
MEblue
MEturquoise
−0.66
(0.01)
0.66
(0.01)
−0.77
(0.002)
0.77
(0.002)
G
Gene significance for MMD
H
HC
MMD
RETNLB
SERPINF2
RETN
MADCAM1
CFD
NTAN1
GPX3
SELL
ADIPOQ
FTMT
SERPINE1
SLC40A1
SELE
B4E1Z4_HUMAN
DIO1
I
Module Membership in turquoise module
Drug
Combined Score
P−value
CFD
GPX3
SELE
SERPINE1
SLC40A1
J
MMD
HC
SERPINE1
BLOC1S1
CFD
C19orf33
NEDD9
NR4A2
RASD1
GPX3
APCDD1
ATF3
IGFBP6
SLC40A1
FKBP5
SELL

Figure 8. Integrated analysis of RNA sequencing and sc-RNAseq of STA samples identified key genes associated with the pathogenesis of MMD.
A, Schematic diagram of the RNA sequencing for STA (MMD = 10, HC = 3). **B**, Volcano plot showing the DEGs between the MMD and HC groups of RNA sequencing. **C**, Dendrogram of gene clustering based on topological overlap matrix dissimilarity. **D**, Venn diagram showing the overlap between 2547 DEGs (turquoise) of RNA sequencing and 82 genes from top 5 DEGs of each cell subpopulation in sc-RNAseq (Top5 gene-cell-deg group). **E**, Determination of soft-thresholding power for weighted correlation network analysis showing scale independence and mean connectivity. **F**, Module–trait relationships showing the correlation between gene modules (MEblue and MEturquoise) and various groups (HC and MMD). **G**, Scatter plot showing the gene significance of MMD vs gene expression. **H**, Protein–protein interaction gene interaction network showing the key gene interactions. Red nodes represent highly correlated nodes, while blue represents moderately connected nodes. **I**, Prediction of drugs interacting with the 5 key genes including *CFD*, *GPX3*, *SERPINE1*, *SELE*, and *SLC40A1*. **J,** Violin plots showing the expression levels of 12 overlapping genes identified from the intersection of bulk RNA sequencing and scRNA-seq data sets. Expression differences between MMD (blue) and HC (red) superficial temporal artery tissues are shown. Black bars indicate the median with interquartile ranges. $^*P < 0.05$. DEG indicates differentially expressed gene; HC, healthy control; MMD, moyamoya disease; sc-RNAseq, single-cell RNA sequencing; and STA, superficial temporal artery.

for MMD, in vitro experimental models are difficult to fully simulate the in vivo case environment of MMD. In the next step of research, the persuasiveness of the experimental results will be enhanced by improving the cell model and increasing the sample size.

CONCLUSIONS

This study provides the first single-cell transcriptomic map of STA tissues from patients with MMD, identifying 8 distinct cellular groups. Our findings highlight the critical roles of ECs, SMCs, and immune cells, particularly NKT cells, in driving vascular remodeling in MMD. We identified interactions between immune cells with vascular ECs or SMCs, which led to cytoskeletal enlargement, enhanced migration and proliferation of ECs and SMCs, and promoted angiogenesis. These effects may contribute to intimal thickening in the diseased arteries of MMD. These findings advance our understanding of MMD pathogenesis and suggest potential therapeutic targets aimed at modulating immune responses to mitigate vascular occlusion in MMD.

ARTICLE INFORMATION

Received January 16, 2025; accepted August 1, 2025.

Affiliations

Department of Neurosurgery, Peking Union Medical College Hospital, Peking Union Medical College and Chinese Academy of Medical Sciences, Beijing, China (S.H., Y.L., C.L., Y.Z.); Department of Neurosurgery, Beijing Tiantan Hospital, Capital Medical University, Beijing, China (J.Z., Z.Z., X.W., Y.W., X.Y.); and, ACROBiosystems Inc, Beijing, China (Z.Q., Y.Z.).

Acknowledgments

The authors thank the health care workers in the department for their help with the project and all participants for their support and cooperation.

Author contributions: Y.L.Z., X.Y,. and S.H.H. conceived and designed the study. S.H.H., J.Z.Z., and Z.Y.Z. performed bioinformatic analysis. S.H.H., J.Z.Z., Z.Y.Z., X.L.W., Y.R.W., Y.T.L., C.X.L., and Z.Q. performed in vitro experiments. S.H.H., Z.Q., and Y.Q.Z. contributed reagents, materials, and analytical tools. All the authors participated in the writing of the manuscript. All authors agree with the content of this study and are responsible for it.

Sources of Funding

This study was supported by National High Level Hospital Clinical Research Funding (2023-PUMCH-E-011), Chinese Academy of Medical Sciences Innovation Fund for Medical Sciences (2023-I2M-C&T-B-048), and the Natural Science Foundation of China (82471337).

Disclosures

The authors declare no competing interests.

Supplemental Material

Data S1
Tables S1–S2
Figures S1–S12

REFERENCES

1. Gonzalez NR, Amin-Hanjani S, Bang OY, Coffey C, Du R, Fierstra J, Fraser JF, Kuroda S, Tietjen GE, Yaghi S, et al. Adult moyamoya disease and syndrome: current perspectives and future directions: a scientific statement from the American Heart Association/American Stroke Association. *Stroke*. 2023;54:e465–e479. doi: 10.1161/STR.0000000000000443
2. Guidelines for diagnosis and treatment of moyamoya disease (spontaneous occlusion of the circle of Willis). *JNm-c*. 2012;52:245–266. doi: 10.2176/nmc.52.245
3. Takagi Y, Kikuta K, Nozaki K, Hashimoto N, Kikuta K-i. Histological features of middle cerebral arteries from patients treated for moyamoya disease. *Neurol Med Chir*. 2007;47:1–4. doi: 10.2176/nmc.47.1
4. Takekawa Y, Umezawa T, Ueno Y, Sawada T, Kobayashi M. Pathological and immunohistochemical findings of an autopsy case of adult moyamoya disease. *Neuropathology*. 2004;24:236–242. doi: 10.1111/j.1440-1789.2004.00550.x
5. Bedini G, Blecharz K, Nava S, Vajkoczy P, Alessandri G, Ranieri M, Acerbi F, Ferroli P, Riva D, Esposito S, et al. Vasculogenic and angiogenic pathways in moyamoya disease. *Curr Med Chem*. 2016;23:315–345. doi: 10.2174/0929867323304160204181543
6. Ihara M, Yamamoto Y, Hattori Y, Liu W, Kobayashi H, Ishiyama H, Yoshimoto T, Miyawaki S, Clausen T, Bang OY, et al. Moyamoya disease: diagnosis and interventions. *Lancet Neurol*. 2022;21:747–758. doi: 10.1016/S1474-4422(22)00165-X
7. Guo DC, Papke CL, Tran-Fadulu V, Regalado ES, Avidan N, Johnson RJ, Kim DH, Pannu H, Willing MC, Sparks E, et al. Mutations in smooth muscle alpha-actin (ACTA2) cause coronary artery disease, stroke, and moyamoya disease, along with thoracic aortic disease. *Am J Hum Genet*. 2009;84:617–627. doi: 10.1016/j.ajhg.2009.04.007
8. He S, Zhang J, Liu Z, Wang Y, Hao X, Wang X, Zhou Z, Ye X, Zhao Y, Zhao Y, et al. Upregulated cytoskeletal proteins promote pathological angiogenesis in moyamoya disease. *Stroke*. 2023;54:3153–3164. doi: 10.1161/STROKEAHA.123.044476
9. Haque A, Engel J, Teichmann SA, Lonnberg T. A practical guide to single-cell RNA-sequencing for biomedical research and clinical applications. *Genome Med*. 2017;9:75. doi: 10.1186/s13073-017-0467-4
10. Kolodziejczyk AA, Kim JK, Svensson V, Marioni JC, Teichmann SA. The technology and biology of single-cell RNA sequencing. *Mol Cell*. 2015;58:610–620. doi: 10.1016/j.molcel.2015.04.005
11. Li Y, Ren P, Dawson A, Vasquez HG, Ageedi W, Zhang C, Luo W, Chen R, Li Y, Kim S, et al. Single-cell transcriptome analysis reveals dynamic

cell populations and differential gene expression patterns in control and aneurysmal human aortic tissue. *Circulation*. 2020;142:1374–1388. doi: 10.1161/CIRCULATIONAHA.120.046528
12. Li Y, Yang J, Huang Y, Ge S, Song X, Jia R, Wang Y. Cellular heterogeneity and immune microenvironment revealed by single-cell transcriptome in venous malformation and cavernous venous malformation. *J Mol Cell Cardiol*. 2022;162:130–143. doi: 10.1016/j.yjmcc.2021.09.004
13. Winkler EA, Kim CN, Ross JM, Garcia JH, Gil E, Oh I, Chen LQ, Wu D, Catapano JS, Raygor K, et al. A single-cell atlas of the normal and malformed human brain vasculature. *Science*. 2022;375:eabi7377. doi: 10.1126/science.abi7377
14. Ren J, Xiao X, Li R, Lv C, Zhang Y, Wang L, Hong T, Zhang H, Wang Y. Single-cell sequencing reveals that endothelial cells, EndMT cells and mural cells contribute to the pathogenesis of cavernous malformations. *Exp Mol Med*. 2023;55:628–642. doi: 10.1038/s12276-023-00962-w
15. Shi J, Yang Y, Cheng A, Xu G, F H. Metabolism of vascular smooth muscle cells in vascular diseases. *Am J Phys Heart Circ Phys*. 2020;319:H613–H631. doi: 10.1152/ajpheart.00220.2020
16. Pan H, Xue C, Auerbach BJ, Fan J, Bashore AC, Cui J, Yang DY, Trignano SB, Liu W, Shi J, et al. Single-cell genomics reveals a novel cell state during smooth muscle cell phenotypic switching and potential therapeutic targets for atherosclerosis in mouse and human. *Circulation*. 2020;142:2060–2075. doi: 10.1161/CIRCULATIONAHA.120.048378
17. Tang Q, Li W, Huang J, Wu Y, Ma C, Tu Y, Zhu Q, Lu J, Xie J, Liu Y, et al. Single-cell sequencing analysis of peripheral blood in patients with moyamoya disease. *Orphanet J Rare Dis*. 2023;18:174. doi: 10.1186/s13023-023-02781-8
18. Kuroda S, Houkin KJTLN. Moyamoya disease: current concepts and future perspectives. *Lancet Neurol*. 2008;7:1056–1066. doi: 10.1016/s1474-4422(08)70240-0
19. Takagi Y, Hermanto Y, Takahashi JC, Funaki T, Kikuchi T, Mineharu Y, Yoshida K, Miyamoto S. Histopathological characteristics of distal middle cerebral artery in adult and pediatric patients with moyamoya disease. *Neurol Med Chir (Tokyo)*. 2016;56:345–349. doi: 10.2176/nmc.oa.2016-0031
20. Mingjun L, Delphine GJATVB. Smooth muscle cell phenotypic diversity. 2019;39. doi: 10.1161/atvbaha.119.312131.
21. Wang A, Li N, Zhang N, Liu J, Yang T, Li D, Li C, Li R, Jiang T, Xia C. Desmoglein-2 affects vascular function in moyamoya disease by interacting with MMP-9 and influencing PI3K signaling. *Mol Neurobiol*. 2024;61:6539–6552. doi: 10.1007/s12035-024-04010-0
22. Xu S, Wei W, Zhang F, Chen T, Dong L, Shi J, Wu X, Zhang T, Li Z, Zhang J, et al. Transcriptomic profiling of intracranial arteries in adult patients with moyamoya disease reveals novel insights into its pathogenesis. *Front Mol Neurosci*. 2022;15:15. doi: 10.3389/fnmol.2022.881954
23. Mertens R, Graupera M, Gerhardt H, Bersano A, Tournier-Lasserve E, Mensah M, Mundlos S, Vajkoczy PJT sr. The genetic basis of moyamoya disease. *Transl Stroke Res*. 2022;13:25–45. doi: 10.1007/s12975-021-00940-2
24. Morito D, Nishikawa K, Hoseki J, Kitamura A, Kotani Y, Kiso K, Kinjo M, Fujiyoshi Y, Nagata K. Moyamoya disease-associated protein mysterin/RNF213 is a novel AAA+ ATPase, which dynamically changes its oligomeric state. *Sci Rep*. 2014;4:4. doi: 10.1038/srep04442
25. Ye F, Niu X, Liang F, Dai Y, Liang J, Li J, Wu X, Zheng H, Qi T, Sheng W. RNF213 loss-of-function promotes pathological angiogenesis in moyamoya disease via the hippo pathway. *Brain*. 2023;146:4674–4689. doi: 10.1093/brain/awad225
26. Ge P, Tao C, Wang W, He Q, Liu C, Zheng Z, Mou S, Zhang B, Liu X, Zhang Q, et al. Circulating immune cell landscape and T-cell abnormalities in patients with moyamoya disease. *Clin Transl Med*. 2024;14:14. doi: 10.1002/ctm2.1647
27. Chen CW, Fu M, Du ZH, Zhao F, Yang WW, Xu LH, Li SL, Ge XY. Long noncoding RNA MRPL23-AS1 promotes adenoid cystic carcinoma lung metastasis. *Cancer Res*. 2020;80:2273–2285. doi: 10.1158/0008-5472.CAN-19-0819
28. Asselman C, Hemelsoet D, Eggermont D, Dermaut B, Impens F. Moyamoya disease emerging as an immune-related angiopathy. *Trends Mol Med*. 2022;28:939–950. doi: 10.1016/j.molmed.2022.08.009
29. Mineharu Y, Miyamoto S. RNF213 and GUCY1A3 in moyamoya disease: key regulators of metabolism, inflammation, and vascular stability. *Front Neurol*. 2021;12:687088. doi: 10.3389/fneur.2021.687088
30. Abumiya T, Fujimura M. Moyamoya vasculopathy and moyamoya-related systemic vasculopathy: a review with histopathological and genetic viewpoints. *Stroke*. 2024;55:1699–1706. doi: 10.1161/strokeaha.124.046999
31. Ivetic A, Hoskins Green HL, Hart SJ. L-selectin: a major regulator of leukocyte adhesion, migration and signaling. *Front Immunol*. 2019;10:1068. doi: 10.3389/fimmu.2019.01068
32. Peng H, Sun R, Tang L, Wei H, Tian Z. CD62L is critical for maturation and accumulation of murine hepatic NK cells in response to viral infection. *J Immunol*. 2013;190:4255–4262. doi: 10.4049/jimmunol.1202395
33. Holman GD. Structure, function and regulation of mammalian glucose transporters of the SLC2 family. *Pflugers Arch*. 2020;472:1155–1175. doi: 10.1007/s00424-020-02411-3
34. Sun B, Chen H, Xue J, Li P, Fu X. The role of GLUT2 in glucose metabolism in multiple organs and tissues. *Mol Biol Rep*. 2023;50:6963–6974. doi: 10.1007/s11033-023-08535-w
35. Burgos M, Gil-Iturbe E, Idoate-Bayón A, Castilla-Madrigal R, Moreno-Aliaga MJ, Lostao MP. The glucose transporter GLUT12, a new actor in obesity and cancer. *J Physiol Biochem*. 2024;81:391–401. doi: 10.1007/s13105-024-01028-9
36. Barron CC, Bilan PJ, Tsakiridis T, Tsiani E. Facilitative glucose transporters: implications for cancer detection, prognosis and treatment. *Metabolism*. 2016;65:124–139. doi: 10.1016/j.metabol.2015.10.007
37. Agam G, Atawna B, Damri O, Azab AN. The role of FKBPs in complex disorders: neuropsychiatric diseases, cancer, and type 2 diabetes mellitus. *Cells*. 2024;13:13. doi: 10.3390/cells13100801
38. Liu N, Li R, Cao J, Song X, Ma W, Liu T, Wang L, Zou J, Zhang B, Liu Z, et al. The inhibition of FKBP5 protects β-cell survival under inflammation stress via AKT/FOXO1 signaling. *Cell Death Dis*. 2023;9:247. doi: 10.1038/s41420-023-01506-x
39. Yao L, Sgadari C, Furuke K, Bloom ET, Teruya-Feldstein J, Tosato G. Contribution of natural killer cells to inhibition of angiogenesis by Interleukin-12. *Blood*. 1999;93:1612–1621. doi: 10.1182/blood.V93.5.1612
40. Ebeling S, Kowalczyk A, Perez-Vazquez D, Mattiola I. Regulation of tumor angiogenesis by the crosstalk between innate immunity and endothelial cells. *Front Oncol*. 2023;13:1171794. doi: 10.3389/fonc.2023.1171794
41. Tyler JC, Pui C, Peter M, Xavier A, Lieve M, Melina E-H, Shuang W, Linhua Z, Ilona K, Gary H, et al. Dendritic cell subsets differentially regulate angiogenesis in human ovarian cancer. 2004;64. doi: 10.1158/0008-5472.Can-04-1272
42. Jacob H, Debra G-W, Yaron H, Inbal A, Caryn G, Shira N-Y, Diana P, Leonor C-D, Tal IA, Irit M, et al. Decidual NK cells regulate key developmental processes at the human fetal-maternal interface. 2006;12. doi: 10.1038/nm1452
43. Belyakova KL, Stepanova OI, Sheveleva AR, Mikhailova VA, Sokolov DI, Sel'kov SA. Interaction of NK cells, trophoblast, and endothelial cells during angiogenesis. *Bull Exp Biol Med*. 2019;167:169–176. doi: 10.1007/s10517-019-04484-2
44. Li X, Ma S, Wang Q, Li Y, Ji X, Liu J, Ma J, Wang Y, Zhang Z, Zhang H, et al. A new integrative analysis of histopathology and single cell RNA-seq reveals the CCL5 mediated T and NK cell interaction with vascular cells in idiopathic pulmonary arterial hypertension. *J Transl Med*. 2024;22:502. doi: 10.1186/s12967-024-05304-6
45. Liu Y, Huang Y, Zhang X, Ma X, He X, Gan C, Zou X, Wang S, Shu K, Lei T, et al. CircZXDC promotes vascular smooth muscle cell Transdifferentiation via regulating miRNA-125a-3p/ABCC6 in moyamoya disease. *Cells*. 2022;11:11. doi: 10.3390/cells11233792
46. Ma X, Huang Y, He X, Zhang X, Liu Y, Yang Y, Yue P, Liu Y, Gan C, Shu K, et al. Endothelial cell-derived let-7c-induced TLR7 activation on smooth muscle cell mediate Vascular Wall remodeling in moyamoya disease. *Transl Stroke Res*. 2023;14:608–623. doi: 10.1007/s12975-022-01088-3